

Map-Free Visual Relocalization Enhanced by Instance Knowledge and Depth Knowledge

Mingyu Xiao^{1,2*}, Runze Chen^{1,2*}, Haiyong Luo^{2†}, Fang Zhao^{1†}, Fan Wu^{1,2}, Hao Xiong^{1,2}, Juan Wang³, Xuepeng Ma³

¹*Beijing University of Posts and Telecommunications, Beijing, China*

²*Institute of Computing Technology, Chinese Academy of Sciences, Beijing, China*

³*Shouguang Cheng Zhi Feng Xing Technology Co., Ltd., ShanDong, China*

{shawnmy,chenrz925,zfsse,wufan98326,xmr2015211989}@bupt.edu.cn, yhluo@ict.ac.cn, sllhjt@139.com,139225785@qq.com

Abstract—Map-free visual relocalization computes camera pose using only a query image and a reference image. Therefore, it is hindered by challenges in feature-point matching and the absence of scale information in monocular images. These issues may cause significant rotational and metric errors, leading to localization failures. To address these challenges, we propose a map-free visual relocalization method enhanced with instance knowledge and depth knowledge. By utilizing instance-based matching, our approach improves the robustness of feature-point matching by focusing on relevant regions across scenes. Additionally, our depth estimation techniques provide reliable depth knowledge from a single image, improving scale recovery and reducing translation errors. Our method surpasses the previous state-of-the-art by 1.071m and 13.593° on the translation error and rotation error, respectively. Furthermore, we are also one of the winners in the Map-free Workshop & Challenge (ECCV2024), underscoring its superiority compared to concurrent approaches.

Index Terms—Map-Free Visual Relocalization, Instance Knowledge, Depth Knowledge

I. INTRODUCTION

Visual relocalization estimates camera position and orientation from a query image, which offers numerous applications such as augmented reality and robotic navigation. Early map-based approaches [1]–[5] rely on image retrieval to estimate poses. Specifically, some methods [6]–[9] designs end-to-end models. Other methods utilize modules that match features [10]–[12], depth estimation [13]–[15] and estimate poses successively. These methods require large image datasets and detailed 3D maps, limiting scalability in memory-constrained environments. Map-free visual relocalization [16], by contrast, computes camera pose using only a query image and a reference image, eliminating the need for pre-built maps. However, it faces challenges due to limitations in feature-point matching and the lack of scale information in monocular images.

To improve the accuracy of map-free relocalization, we propose a novel framework that not only enhances matching precision but also effectively addresses the challenges of metric depth estimation. Our approach significantly advances visual relocalization by systematically reducing both rotation and translation errors, which are critical for achieving reliable localization without the need for pre-existing maps. To

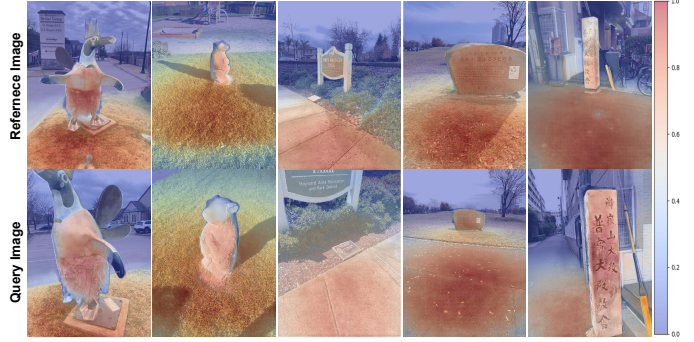


Fig. 1. The matched points foreground objects exhibit slightly higher confidence, but this preference is not significant.

reduce the rotation errors, we delve into a powerful Multi-view stereo reconstruction model DUS3R [17], which can obtain pairwise pointmaps based on the extracted 3D features from two images. Despite DUS3R's good matching ability, its performance on map-free visual relocalization remains suboptimal. To investigate this, we visualize the confidence of the pointmaps between the reference and query frames in Figure 1. Points closer to red indicate higher confidence, while those nearer to blue show lower confidence. As illustrated in Figure 1, some foreground objects exhibit slightly higher confidence, but this preference is not significant. However, in map-free visual relocalization tasks, accurate matching of foreground objects is crucial for successful relocalization, because foreground objects are more robust features in the global scene, making them more conducive to precise relocalization. The lack of significant confidence in the foreground object areas explains why DUS3R performs well in multi-view stereo reconstruction but struggles with map-free visual relocalization. Thereby, to fully utilize the matching ability of DUS3R, we introduce a feature point matching method enhanced by instance knowledge, which restricts the matching scope to within specific instances. By guiding the model to focus on specific instance matches, we can effectively reduce incorrect matches between different objects.

To reduce translation errors, our framework incorporates

* These authors contributed equally to this work.

† Corresponding authors: Haiyong Luo and Fang Zhao.

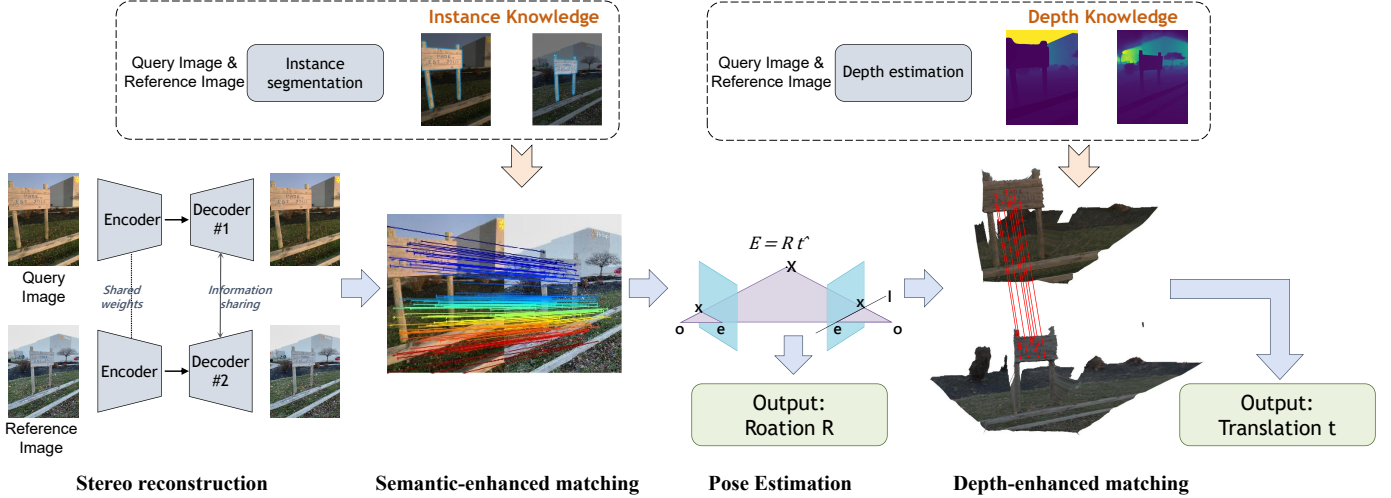


Fig. 2. Overview. Our model first takes two input images as input and obtains aligned point maps. Then, utilizing instance segmentation knowledge, feature points are matched both globally and within identified masks. The matched points are then input into an essential matrix solver, which computes the rotation matrix R and a scale-free translation vector \bar{t} . Subsequently, depth knowledge is applied to project the feature points into 3D space, allowing for the recovery of a scaled translation vector t .

Metric3D [18], which employs standard camera transformations and joint depth-normal optimization to tackle the metric depth estimation problem from a single image. As our framework requires depth information to recover the scale of the translation vector, accurate scale recovery can achieve better translation accuracy. Our method achieves the best results on the map-free visual relocalization dataset compared to all methods mentioned in [16], highlighting the effectiveness of our method. Our contributions are as follows:

- We proposed a hierarchical matching method that integrates instance-level and feature-level matching, effectively combining the advantages of global instance-level semantic matching and local feature point-based matching. This approach improves the accuracy of relocalization in map-less scenarios, with instance-level matching enhancing the precision of global alignment.
- We conducted extensive experiments on complex scenarios within the map-free visual relocalization dataset, which includes spatiotemporal differences and significant parallax. These experiments demonstrate that our method exhibits superior generalization performance, surpassing existing algorithms.

II. METHOD

The overall framework of our method is shown in Figure 2. We leverage instance knowledge to enhance the feature point matching and depth knowledge to facilitate scale recovery.

A. Instance-enhanced Matching

We utilize DUST3R [17] to perform feature point matching by processing two input images I_1 and I_2 , and outputs the corresponding point maps X_1 and X_2 . Then, the nearest neighbor matching and reciprocal matching are utilized to find the matching point. Firstly, we use the nearest neighbor

search in the 3D point map space. For each pixel (i, j) in image I_1 , we first find the corresponding 3D point $X_{1,1}(i, j)$ in $X_{1,1}$. Then we perform a nearest neighbor search in $X_{2,1}$ to localize the 3D point $X_{2,1}(k, l)$ that is closest to $X_{1,1}(i, j)$, where (k, l) are the coordinates of the matching point found in $X_{2,1}$. Then, we use reciprocal matching to improve the accuracy of the matching. From each pixel (i, j) in I_1 , we find the matching point (k, l) in I_2 . Simultaneously, from each pixel (k, l) in I_2 , we find the matching point (i, j) in I_1 . A match is considered valid only if the results are consistent in both directions, i.e., $(i, j) \rightarrow (k, l)$ and $(k, l) \rightarrow (i, j)$. We denote the global mapping as $Map^g = \{((i_1, j_1), (k_1, l_1)), ((i_2, j_2), (k_2, l_2)), \dots, ((i_n, j_n), (k_n, l_n))\}$, where each tuple in the map represents the matching relation between points in I_1 and I_2 , we define the $\mathcal{M}()$ as the feature point matching method:

$$Map^g = \mathcal{M}(I_1, I_2, X_{1,1}, X_{2,1}), \quad (1)$$

where the Map^g is the correspondences in global area. To significantly enhance the precision of feature point matching, instance segmentation technology is integrated, enabling the accurate extraction of primary objects from images and focusing on matching within identical instance objects. Specifically, we use SegGPT [19] to segment the same object in both the reference and query images. The masks for the o -th object are denoted as $Mask_1^o$ for the reference frame and $Mask_2^o$ for the query frame, respectively. Then, our feature point matching algorithm conducts refined matching within these masks. Specifically, for the object o , we denote corresponding image as I_1^o and I_2^o , where $I_1^o = I_1 \odot Mask_1^o$, $I_2^o = I_2 \odot Mask_2^o$. Then, we perform point map reconstruction within the object and obtain corresponding point maps $X_{1,1}^o$ and $X_{2,1}^o$. Finally,

we conduct matching within the mask object area:

$$Map^o = \mathcal{M}(I_1^o, I_2^o, X_{1,1}^o, X_{2,1}^o), \quad (2)$$

where the Map^o is the correspondences in the same object. This modification aims for more precise matching within individual instances, ensuring that the feature-matching process is restricted to relevant areas defined by the instance masks. Finally, for areas of instance object, we use Map^o . For background areas, we use Map^g :

$$Map = \begin{cases} Map^o & \text{if is instance object,} \\ Map^g & \text{else} \end{cases} \quad (3)$$

B. Pose Estimation

We selected the 5-point algorithm [20] combined with the essential matrix [21] to compute the essential matrix E from matched point pairs:

$$E = U\Sigma V^T, \quad (4)$$

where U and V are orthogonal matrices representing rotation or reflection, and Σ is a diagonal matrix representing the original matrix's stretching factor. The matrix E is then decomposed into the rotation matrix R and the scale-free translation vector \bar{t} :

$$E = \bar{t} \times R. \quad (5)$$

C. Depth-enhanced Scale Recovery

We use Metric3D [18] for scale recovery. The input image I is initially transformed into a canonical camera space image I_c , which is then processed through an encoder-decoder network to predict a depth d_c . Finally, the predicted canonical depth d_c is converted back to the actual depth d in the original camera space by scaling d_c using the ratio ω_d , i.e., $d = \omega_d d_c$.

To integrate depth information into matching, we combine the depth estimation results d_1, d_2 with matching point pairs Map from the instance-enhanced matching process. Assuming that the coordinates of a feature point pair in the reference image are (i_1, j_1) , and those of the corresponding feature point pair in the query image are (k_1, l_1) , we can calculate their 3D coordinates assisted with depth values d_1 and d_2 :

$$p_1 = d_1 \cdot K^{-1} \begin{bmatrix} i_1 \\ j_1 \\ 1 \end{bmatrix} \quad p_2 = d_2 \cdot K^{-1} \begin{bmatrix} k_1 \\ l_1 \\ 1 \end{bmatrix}, \quad (6)$$

where K represents the camera parameter matrix. p_1 and p_2 represents their corresponding 3D coordinates. For each pair of 3D-3D correspondences, we compute a scale factor s of the translation vector:

$$s = \frac{\|p_1 - Rp_2\|}{\|\bar{t}\|}, \quad (7)$$

where $\|p_1 - Rp_2\|$ denotes the distance difference between 3D points in two images, and $\|\bar{t}\|$ is the length of the translation vector. After obtaining the scales between different point pairs, we use the RANSAC algorithm [22] to select the one with the highest agreement as the final scale factor. Finally, we transform the scale-free translation vector \bar{t} to the scaled

translation vector $t = s \times \bar{t}$. Combining t with the rotation matrix R to form the final relative pose of the query image with respect to the reference image. Combining the translation vector t with the rotation matrix R yields the final relative pose of the query image with respect to the reference image.

Algorithm 1: INFERENCE

```

1 Input: Two input images,  $I_1$  and  $I_2$ .
2 Output: Rotation matrix  $R$  and translation vector  $t$ .
3 // Point Map Reconstruction
4 calculate  $X_{1,1}$  and  $X_{2,1}$  based on  $I_1$  and  $I_2$ ;
5 // Instance-enhanced Matching
6  $Mask_1, Mask_2 \leftarrow SegGPT(I_1, I_2)$ ;
7  $Map^g = \mathcal{M}(I_1, I_2, X_{1,1}, X_{2,1})$ ;
8  $Map^o = \mathcal{M}(I_1^o, I_2^o, X_{1,1}^o, X_{2,1}^o)$ 
9 calculate  $Map$  based on Eq. 3;
10 // Pose Estimation
11 compute the rotation matrix  $R$  and the scale-free unit
12 vector  $\bar{t}$  based on Eq. 4 and 5;
13 // Depth-enhanced Matching
14 calculate depth  $d_1, d_2$  of  $I_1, I_2$  based on [18];
15 project matching points into 3D space based on Eq. 6;
16 calculate scale  $s$  based on Eq. 7;
17 recovery scaled translation vector  $t$ ;
18 Return  $R, t$ .

```

III. EXPERIMENT

We evaluate our method using the map-free visual relocalization dataset [16], following the evaluation protocol outlined by Arnold *et al.* [16].

A. Main Results

We analyze current models for insights into better relocalization algorithms. Specifically, we build the comparison method using three components: feature matching methods (SIFT [23], LoFTR [24], and SuperGlue [11]), depth estimation (DPT [25] fine-tuned on KITTI [26] and NYUv2 [27]), and pose estimation (5-point solver [20] with MAGSAC++ [28], PNP [29], and Procrustes [30]). Additionally, we compare various end-to-end methods, including RPR[3D-3D]. By combining these components and end-to-end methods, we obtain 13 comparison methods.

As shown in Table I, the results show that our method achieves a significant reduction in Average Median Pose Error. For example, the RPR[3D-3D] method, which performs best among existing methods, has an Average Median Rotation Error of 22.623° , while our method achieves 9.030° . This improvement is largely due to our advanced feature point matching technique, which retains global matching information while focusing on instance-level matching. This approach reduces significant matching errors and enhances precise local matching. For Average Median Translation Error, the RPR[3D-3D] method reports an error of 1.667m , whereas our method achieves 0.596m . For the other three metrics, the Average

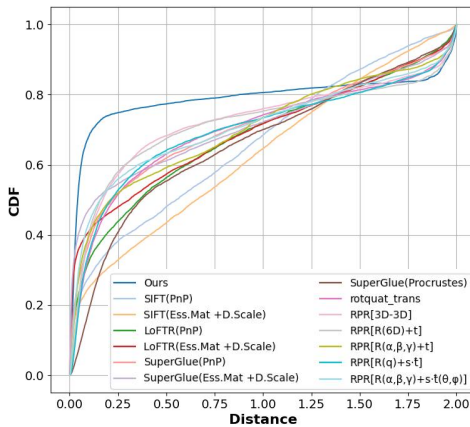
TABLE I
QUANTITATIVE COMPARISONS. OUR APPROACH OUTPERFORMS COMPARISON METHODS.

Method	Average Translation Error(m)(↓)	Average Rotation Error(°)(↓)	Average Reprojection Error(px)(↓)	Precision @ VCRE < 90px (↑)	AUC @ VCRE < 90px (↑)
SIFT (PnP)	3.722	72.291	207.306	0.208	0.396
SIFT (Ess.Mat +D.Scale)	3.331	74.448	234.170	0.187	0.395
LoFTR (PnP)	2.665	49.212	178.491	0.283	0.569
LoFTR (Ess.Mat + D.Scale)	2.578	43.522	180.556	0.301	0.581
SuperGlue (Procrustes)	2.882	55.455	210.779	0.210	0.388
SuperGlue (PnP)	2.379	42.269	173.012	0.311	0.541
SuperGlue (Ess.Mat +D.Scale)	2.188	36.358	178.542	0.321	0.563
RPR [$R(\alpha, \beta, \gamma) + \hat{t}$]	2.543	33.977	215.479	0.261	0.261
RPR [$R(q) + t$]	2.370	32.390	169.204	0.290	0.290
RPR [$R(q) + s \cdot \hat{t}$]	2.125	31.772	172.098	0.284	0.284
RPR [$R(6D) + t$]	1.845	24.172	163.199	0.333	0.333
RPR [$R(\alpha, \beta, \gamma) + s \cdot \hat{t}(\theta, \phi)$]	1.764	25.349	178.918	0.336	0.336
RPR [3D-3D]	<u>1.667</u>	<u>22.623</u>	<u>158.017</u>	<u>0.346</u>	<u>0.346</u>
Ours	0.596	9.030	70.439	0.484	0.591

Median Reprojection Error indicates the overall geometric accuracy of the error. Precision@VCRE < 90px evaluates the success rate under a specific threshold, emphasizing the algorithm's performance within a defined error range. Meanwhile, AUC@VCRE < 90px is a global assessment metric that examines performance across various error thresholds, reflecting the robustness and stability of the algorithm. Our method outperforms all baselines in these metrics, demonstrating the robustness and effectiveness of our approach.

We evaluate our method's effectiveness against the baseline by computing the Cumulative Distribution Function (CDF) for pose estimation errors across all scenes (Figure 3). The CDF illustrates the cumulative probability of errors, with a steeper rise towards 1 at lower error values indicating better performance. Our method's CDF shows a quicker ascent at reduced error levels compared to the baseline, demonstrating its consistently lower pose estimation errors and superior robustness and accuracy across various scenarios.

Fig. 3. The CDF poses estimation errors across all scenes.



B. Ablation Study

In this section, we conduct extensive ablation studies to investigate the significance of instance and depth knowledge within our framework.

1) *Instance Knowledge*: We ablate our instance knowledge and keep all other components unchanged (third line). As

shown in Table II, when instance knowledge is removed, both rotation and translation errors increase. This may be because the absence of accurate feature point matching introduces significant errors when calculating the essential matrix.

2) *Depth Knowledge*: As directly removing the depth estimation module would cause the model to be unable to output poses, we analyze the importance of depth knowledge by replacing our depth estimation method with DPT [25]. Notably, DPT [25] has been shown to perform better than other depth estimation models in previous experiments [16]. As shown in the fourth line in Table II, removing our depth knowledge resulted in a noticeable increase in Median Trans. Error. This is because better depth knowledge enables more accurate scale recovery.

Additionally, we remove both instance and depth knowledge, which is effectively equivalent to DUSt3R [17]. As shown in the last line in Table II, this results in a significant increase in both Median Rot. Error and Median Trans. Error, further emphasizing the importance of instance knowledge and depth knowledge.

TABLE II
ABLATION STUDY

Instance	Depth	Median Trans. Error	Median Rot. Error	Median Reproj. Error
✓	✓	0.596	9.030	70.439
	✓	2.343	43.522	155.883
		0.918	9.030	116.146
		3.291	60.093	266.326

IV. CONCLUSION

We propose a novel map-free relocalization method that estimates the relative pose of a query frame using reference and query images. By leveraging instance segmentation to guide feature point matching within objects, our approach reduces incorrect matches and enhances accuracy. Furthermore, we optimize 3D point coordinates through depth estimation for improved scale recovery. Extensive experiments validate the effectiveness of our collaborative knowledge-enhanced visual relocalization, offering promising advancements in map-free relocalization accuracy.

REFERENCES

- [1] L. Svärm, O. Enqvist, F. Kahl, and M. Oskarsson, “City-scale localization for cameras with known vertical direction,” *Transactions on Pattern Analysis and Machine Intelligence*, 2016.
- [2] Y. Li, N. Snavely, D. Huttenlocher, and P. Fua, “Worldwide pose estimation using 3d point clouds,” in *European Conference on Computer Vision*, 2012.
- [3] E. Brachmann and C. Rother, “Visual camera re-localization from rgb and rgb-d images using dsac,” *Transactions on Pattern Analysis and Machine Intelligence*, 2021.
- [4] V. Panek, Z. Kukelova, and T. Sattler, “Visual localization using imperfect 3d models from the internet,” in *Computer Vision and Pattern Recognition Conference*, 2023.
- [5] M. Kim, J. Koo, and G. Kim, “Ep2p-loc: End-to-end 3d point to 2d pixel localization for large-scale visual localization,” in *International Conference on Computer Vision*, 2023.
- [6] Y. Shavit, R. Ferens, and Y. Keller, “Learning multi-scene absolute pose regression with transformers,” in *International Conference on Computer Vision*, 2021.
- [7] Z. Laskar, I. Melekhov, S. Kalia, and J. Kannala, “Camera relocalization by computing pairwise relative poses using convolutional neural network,” in *International Conference on Computer Vision Workshop*, 2017.
- [8] A. Kendall and R. Cipolla, “Modelling uncertainty in deep learning for camera relocalization,” in *International Conference on Robotics and Automation*, 2016.
- [9] S. Brahmbhatt, J. Gu, K. Kim, J. Hays, and J. Kautz, “Geometry-aware learning of maps for camera localization,” in *Computer Vision and Pattern Recognition Conference*, 2018.
- [10] J. Sun, Z. Shen, Y. Wang, H. Bao, and X. Zhou, “LoFTR: Detector-free local feature matching with transformers,” in *Computer Vision and Pattern Recognition Conference*, 2021.
- [11] P.-E. Sarlin, D. DeTone, T. Malisiewicz, and A. Rabinovich, “Superglue: Learning feature matching with graph neural networks,” in *Computer Vision and Pattern Recognition Conference*, 2020.
- [12] D. G. Lowe, “Distinctive image features from scale-invariant keypoints,” *International Journal of Computer Vision*, 2004.
- [13] Y. Wu, Y. Heng, M. Niranjan, and H. Kim, “Depth estimation for a single omnidirectional image with reversed-gradient warming-up thresholds discriminator,” in *International Conference on Acoustics, Speech and Signal Processing*, 2023.
- [14] D. Miao, F.-P. Tian, and W. Feng, “Active camera relocalization with rgbd camera from a single 2d image,” in *International Conference on Acoustics, Speech and Signal Processing*, 2018.
- [15] W.-Y. Lo, C.-T. Chiu, and J.-Y. Luo, “Depth estimation from single image through multi-path-multi-rate diverse feature extractor,” in *International Conference on Acoustics, Speech and Signal Processing*, 2020.
- [16] E. Arnold, J. Wynn, S. Vicente, G. Garcia-Hernando, A. Monszpart, V. Prisacariu, D. Turmukhambetov, and E. Brachmann, “Map-free visual relocalization: Metric pose relative to a single image,” in *European Conference on Computer Vision*, 2022.
- [17] S. Wang, V. Leroy, Y. Cabon, B. Chidlovskii, and J. Revaud, “Dust3r: Geometric 3d vision made easy,” in *Computer Vision and Pattern Recognition Conference*, 2024.
- [18] M. Hu, W. Yin, C. Zhang, Z. Cai, X. Long, H. Chen, K. Wang, G. Yu, C. Shen, and S. Shen, “Metric3d v2: A versatile monocular geometric foundation model for zero-shot metric depth and surface normal estimation,” *arXiv preprint arXiv:2404.15506*, 2024.
- [19] X. Wang, X. Zhang, Y. Cao, W. Wang, C. Shen, and T. Huang, “Seggp: Segmenting everything in context,” *arXiv preprint arXiv:2304.03284*, 2023.
- [20] D. Nistér, “An efficient solution to the five-point relative pose problem,” *Transactions on Pattern Analysis and Machine Intelligence*, 2004.
- [21] R. Hartley and A. Zisserman, *Multiple view geometry in computer vision*. Cambridge university press, 2003.
- [22] M. A. Fischler and R. C. Bolles, “Random sample consensus: a paradigm for model fitting with applications to image analysis and automated cartography,” *Communications of the ACM*, 1981.
- [23] D. G. Lowe, “Distinctive image features from scale-invariant keypoints,” *International Journal of Computer Vision*, 2004.
- [24] J. Sun, Z. Shen, Y. Wang, H. Bao, and X. Zhou, “LoFTR: Detector-free local feature matching with transformers,” in *Computer Vision and Pattern Recognition Conference*, 2021.
- [25] R. Ranftl, A. Bochkovskiy, and V. Koltun, “Vision transformers for dense prediction,” in *International Conference on Computer Vision*, 2021.
- [26] A. Geiger, P. Lenz, and R. Urtasun, “Are we ready for autonomous driving? the kitti vision benchmark suite,” in *Computer Vision and Pattern Recognition Conference*, 2012.
- [27] N. Silberman, D. Hoiem, P. Kohli, and R. Fergus, “Indoor segmentation and support inference from rgbd images,” in *European Conference on Computer Vision*, 2012.
- [28] D. Barath, J. Noskova, M. Ivashchkin, and J. Matas, “Magsac++, a fast, reliable and accurate robust estimator,” in *Computer Vision and Pattern Recognition Conference*, 2020.
- [29] X.-S. Gao, X.-R. Hou, J. Tang, and H.-F. Cheng, “Complete solution classification for the perspective-three-point problem,” *Transactions on Pattern Analysis and Machine Intelligence*, 2003.
- [30] D. W. Eggert, A. Lorusso, and R. B. Fisher, “Estimating 3-d rigid body transformations: a comparison of four major algorithms,” *International Conference on Machine Vision Applications*, 1997.